Modeling and Simulation for Bifurcations of SSR in Large Wind Farms

Majdi M. Alomari*‡, Mohammad Sabati*, Mohammad S. Widyan**, and Nafesah I. Alshdaifat***

*Electrical Engineering Dept., School of Engineering, Australian College of Kuwait, 13015 Safat, KUWAIT
**Electrical Engineering Dept., Faculty of Engineering, Hashemite University,
13115 Zarqa, JORDAN
***Department of Renewable Energy Engineering, Faculty of Engineering, Middle East University, 11831 Amman, JORDAN

(m.alomari@ack.edu.kw, m.sabati@ack.edu.kw, mohammadwidyan@hu.edu.jo, nafesah58@gmail.com)

‡ Majdi M. Alomari, P.O. Box 1411, Safat - 13015, Kuwait, Tel: +965 96088966, m.alomari@ack.edu.kw

Received: 21.01.2017 Accepted:26.04.2017

Abstract- Bifurcations of subsynchronous resonance (SSR) is applied to wind farms which depends on induction generators (IG). Series compensated transmission lines are connected to these wind farms. The developed IEEE second benchmark model (first system) of SSR is assumed. The system studied is presented as a set of equations. The type of these equations are nonlinear ordinary differential equations from the first order level. The compensation factor is applied as a control parameter. Therefore, bifurcation theory can be used in the considered nonlinear system. The impress of both torsional interaction and induction generator effect are considered. Bifurcations of SSR are studied for an enormous range of series compensation values in the cases of various sizes of wind farms and various wind farm power outputs. The results show that Hopf bifurcations may occur in large wind farms which consists of double-cage IGs at high value of compensation. Once the wind farm size is increased, the Hopf bifurcation point initially shifts to the left at a less value of compensation then shifts to the right at a larger value of compensation with a supercritical Hopf bifurcation remains in all cases. This resulted in only quantitative changes in Hopf bifurcation for the case of changing the wind farm size. Additionally, when the a large wind farm power output increases the Hopf bifurcation point shifts a little to the left at a slightly less value of compensation. On the contrary, the type of Hopf bifurcation changes from subcritical to supercritical. Therefore, the influence of the variation in the wind farm size on bifurcation is only of a quantitative change, while the impact of variation in the power output is mainly a qualitative change.

Keywords- Hopf Bifurcation, Wind Turbine, Induction Generator, Subsynchronous Resonance.

1. Introduction

One of the major concerns in the field of energy is possible energy shortage and an environmental pollution. For these reasons, utilization of wind energy to generate electricity is rapidly growing and has attracted significant attention worldwide. Wind power technology is spreading quickly in renewable energy generation systems [1] - [7]. Therefore, with the rapid growth of wind farm installed capacity, the large wind turbine generators (WTGs) are widely utilized into power system networks. In the recent years, the wind energy industry is considered as the most significant section of renewable energy industries, in which design developments and improved technology have made the wind energy in rapidly increasing levels of their penetration. Examples of such recent advancements include: increase in wind turbines size while decreasing their cost and improvement of the controllability of the wind power plants. Furthermore, the progress in power electronics field introduced wind energy as a significant and achievable source in renewable energy sector [8] - [12].

The mechanical drive train system, in a commercially operated wind farms, transmits the rotor torque and feeds it to the electrical generator. Among several renewable energy sources as aforementioned, wind power is the fastest developing one. Consequently, providing high-performance, reliable, and efficient wind power generation is a practical and important concern in the power industry.

Series capacitive compensation is an efficient method to enhance the power system stability and power transfer ability mainly when large values of power is transmitted through

long transmission lines. An effective technique to increase the power transfer ability and improve the system stability is the series capacitive compensation. However, this compensation can result a major problem named subsynchronous resonance (SSR) in power system networks [13]-[15]. In SSR, oscillating torsional torques is produced by the interaction of the mechanical oscillation modes of the turbine-generator set with the electrical oscillation modes of the series compensated transmission lines [16].

The incidence of different categories of bifurcation in power system networks has been verified. Hopf bifurcation is the most frequently type of bifurcation in these networks which takes place once a complex conjugate pair of eigenvalue of the linearized system about the equilibrium condition transversely crosses the imaginary axis of complex plane [17]. The occurrence of limited cycles from a fixed point leads to oscillations, which possibly go through complicated situation of bifurcations such as crises, cyclic folds, or period multiplication.

Pourbeik *et. al.* [18] studied both doubly fed induction generator (DFIG) in addition to conventional induction generator (IG) based wind farms. For the first time, they investigated the interaction of wind farm including series compensated transmission line. Induction generator effect was verified in the case of adding the series capacitor depending on the simulation studies with squirrel cage IG-based wind farms. Ostadi *et. al.* [19] introduced a model of wind farm depends on DFIG which linked with a series compensated line. They presented a time-domain simulations and small signal analysis. Furthermore, they studied the effect of a control parameters and series capacitor on the SSR power system. Additional research on SSR in wind farms including DFIG was presented. A complete model of this system has been described [20]-[27]. The authors introduced a time-history simulation and a small signal analysis to study the SSR conditions.

In this paper, power system dynamics is applied employing a nonlinear dynamics technique, which utilizes the bifurcation theory to examine the complex dynamics of the studied power system [28]. The power system changes the stability through Hopf bifurcation point and then a limit cycle is born near this point. This bifurcation is classified as supercritical when the limit cycle is stable and subcritical when it is unstable. The Hopf bifurcation type can be obtained using numerical integration of the model after applying small value of initial disturbances slightly after and before the HB point. In this research, the effect of the wind power output, size of wind farm, and value of series compensation on bifurcation have been studied.

The rest of this study is planned in the following order: section 2 shows the description of the combined electrical and mechanical system under investigation. In section 3, the complete dynamical nonlinear mathematical model is stated. The numerical simulations accompanied with discussions and results are summarized, in section 4. Finally, conclusions are condensed in section 5.

2. System Description

The modified IEEE second benchmark model (first system) of SSR is considered [29], shown in Figure 1. The power system is a large squirrel cage induction generator considered wind farms linked with series compensated lines. Figure 2 shows a standard two-mass drive train system [30]-[32]. The two masses are one for the combined mass of hub and three blades in addition to the second mass for the generator rotor.

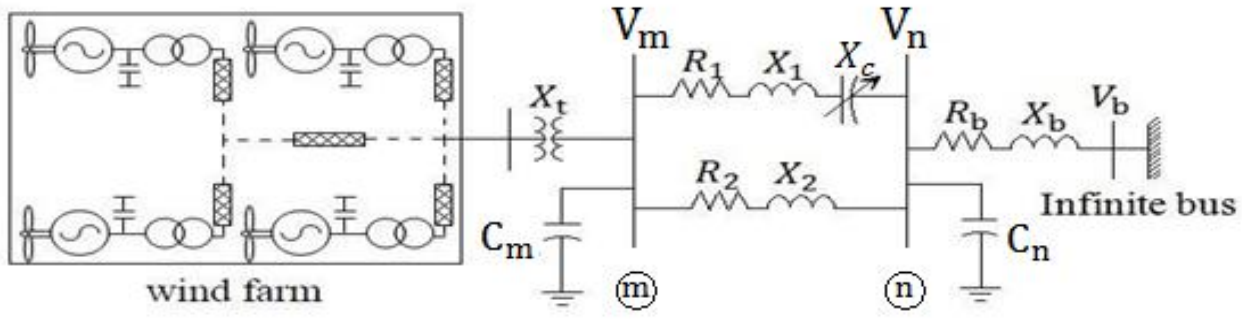

Fig. 1. Electrical system (modified version of first system of the IEEE second benchmark model of SSR)

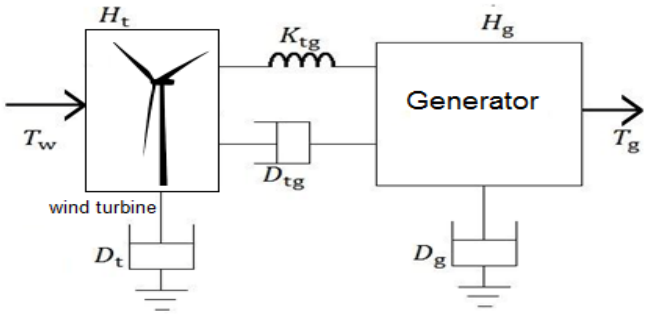

Fig. 2. Two-mass drive train system

Where D is the damping coefficient, H is the inertia constant, K is the Shaft stiffness, T_g is the electromagnetic torque output of generator, and T_W is the mechanical torque input to wind turbine.

3. Mathematical Model

To start with modeling, the system under study is separated into two subsystems; wind farm and compensated transmission line. The wind farm is subdivided further into two subsystems; electrical generator and mechanical drive train. In fact, the electrical system consist of the dynamical nonlinear mathematical description of a double-cage induction generator and the transmission line [31], [32]. Therefore, the dynamic models of mechanical drive train, double-cage induction generator and the network equations will be presented.

The generator model considered for this system includes six equations; *d-q* coordinates of stator current, *d-q* components of first-cage induced rotor voltages, and *d-q* coordinates of second-cage induced rotor voltages equations. In mechanical system, each mass can be described as a second order ordinary differential equation. This equation is also called swing equation which can be rewritten as two equations with first order ordinary differential type. Therefore, the full mathematical system that depicts the dynamics of the system is described as follows (all parameters are defined in Appendix A) [29]:

3.1 The two-mass drive train system:

In the two-mass system, first mass indicates the combined mass of hub and three blades while the second mass indicates the generator rotor linked with the shaft. This subsystem can be modeled as:

$$\dot{\omega}_t = \frac{-D_{tg}}{2H_t}\,\omega_t + \frac{-K_{tg}}{2H_t}\,\delta_{tg} + \frac{D_{tg}}{2H_t}\,\omega_g + \frac{1}{2H_t}\,T_w \quad (1)$$

$$\dot{\delta}_{tg} = \omega_t - \omega_g \quad (2)$$

$$\dot{\omega}_g = \frac{D_{tg}}{2H_g}\,\omega_t + \frac{K_{tg}}{2H_g}\,\delta_{tg} - \frac{D_{tg}}{2H_g}\,\omega_g + \frac{1}{2H_g}\,E_{d1}\,I_{ds} + \frac{1}{2H_g}\,I_{qs}\,E_{q1} \quad (3)$$

3.2 Induction generator equations:

The wind farm considered in this study consists of 300 identical double cage induction generators (IGs). All generators are subjected to the same wind speed and have the same size (2 MW) totaling to an equivalent single 600 MW induction generator [33]. A per unit system of an IG in the synchronously rotating *d-q* coordinates is presented. Consequently, the dynamic equations of the IG can be modeled as follows:

$$\dot{I}_{ds} = \frac{-R_s\,\omega_s}{X_o}\,I_{ds} + \omega_s\,I_{qs} - \frac{\omega_s}{X_o}\,E_{d1} - \frac{\omega_s}{X_o}\,V_{ds} - \frac{1}{X_o}\left[\frac{-\omega_s\,R_{r1}}{X_r}\left(X_{r2}\,E_{q1} - X_m\,X_{ro2}\,E_{q2} - \frac{(X_m\,X_{ro2})^2}{X_r}\,I_{ds}\right) - S\,\omega_s\,E_{d1}\right] \quad (4)$$

$$\dot{I}_{qs} = \frac{-R_s\,\omega_s}{X_o}\,I_{qs} - \omega_s\,I_{ds} - \frac{\omega_s}{X_o}\,E_{q1} - \frac{\omega_s}{X_o}\,V_{qs} + \frac{1}{X_o}\left[\frac{-\omega_s\,R_{r1}}{X_r}\left(X_{r2}\,E_{d1} - X_m\,X_{ro2}\,E_{d2} + \frac{(X_m\,X_{ro2})^2}{X_r}\,I_{qs}\right) + S\,\omega_s\,E_{q1}\right] \quad (5)$$

$$\dot{E}_{d1} = \frac{-\omega_s\,R_{r1}}{X_r}\left(X_{r2}\,E_{d1} - X_m\,X_{ro2}\,E_{d2} + \frac{(X_m\,X_{ro2})^2}{X_r}\,I_{qs}\right) + S\,\omega_s\,E_{q1} \quad (6)$$

$$\dot{E}_{q1} = \frac{-\omega_s\,R_{r1}}{X_r}\left(X_{r2}\,E_{q1} - X_m\,X_{ro2}\,E_{q2} - \frac{(X_m\,X_{ro2})^2}{X_r}\,I_{ds}\right) - S\,\omega_s\,E_{d1} \quad (7)$$

$$\dot{E}_{d2} = \frac{-\omega_s\,R_{r2}}{X_r}\left(\frac{-X_{1\_2}{}^2}{X_m\,X_{ro2}}\,E_{d1} + X_{1\_2}\,E_{d2}\right) + S\,\omega_s\,E_{q2} \quad (8)$$

$$\dot{E}_{q2} = \frac{-\omega_s\,R_{r2}}{X_r}\left(\frac{-X_{1\_2}{}^2}{X_m\,X_{ro2}}\,E_{q1} + X_{1\_2}\,E_{q2}\right) - S\,\omega_s\,E_{d2} \quad (9)$$

3.3 Transmission lines (network) equations:

In this subsystem, the ac transmission lines are modified from the IEEE second benchmark model (first system) of SSR [29]. The dynamic equations of the transmission lines including the series capacitor in *d-q* coordinates can be described as:

$$\dot{V}_{ds} = \frac{1}{C_g} I_{ds} + \omega_s V_{qs} - \frac{1}{C_g} I_d \quad (10)$$

$$\dot{V}_{qs} = \frac{1}{C_g} I_{qs} - \omega_s V_{ds} - \frac{1}{C_g} I_q \quad (11)$$

$$\dot{I}_d = \frac{1}{L_t} V_{ds} + \omega_s I_q - \frac{R_t}{L_t} I_d - \frac{1}{L_t} V_{md} \quad (12)$$

$$\dot{I}_q = \frac{1}{L_t} V_{qs} - \omega_s I_d - \frac{R_t}{L_t} I_q - \frac{1}{L_t} V_{mq} \quad (13)$$

$$\dot{I}_{d1} = \frac{1}{L_1} V_{md} + \omega_s I_{q1} - \frac{R_1}{L_1} I_{d1} - \frac{1}{L_1} V_{cd} - \frac{1}{L_1} V_{nd} \quad (14)$$

$$\dot{I}_{q1} = \frac{1}{L_1} V_{mq} - \omega_s I_{d1} - \frac{R_1}{L_1} I_{q1} - \frac{1}{L_1} V_{cq} - \frac{1}{L_1} V_{nq} \quad (15)$$

$$\dot{I}_{d2} = \frac{1}{L_2} V_{md} + \omega_s I_{q2} - \frac{R_2}{L_2} I_{d2} - \frac{1}{L_2} V_{nd} \quad (16)$$

$$\dot{I}_{q2} = \frac{1}{L_2} V_{mq} - \omega_s I_{d2} - \frac{R_2}{L_2} I_{q2} - \frac{1}{L_2} V_{nq} \quad (17)$$

$$\dot{V}_{md} = \frac{1}{C_m} I_d - \frac{1}{C_m} I_{d1} - \frac{1}{C_m} I_{d2} + \omega_s V_{mq} \quad (18)$$

$$\dot{V}_{mq} = \frac{1}{C_m} I_q - \frac{1}{C_m} I_{q1} - \frac{1}{C_m} I_{q2} - \omega_s V_{md} \quad (19)$$

$$\dot{V}_{nd} = \frac{1}{C_n} I_{d1} + \frac{1}{C_n} I_{d2} + \omega_s V_{nq} - \frac{1}{C_n} I_{bd} \quad (20)$$

$$\dot{V}_{nq} = \frac{1}{C_n} I_{q1} + \frac{1}{C_n} I_{q2} - \omega_s V_{nd} - \frac{1}{C_n} I_{bq} \quad (21)$$

$$\dot{I}_{bd} = \frac{1}{L_b} V_{nd} - \frac{R_b}{L_b} I_{bd} + \omega_s I_{bq} - \frac{1}{L_b} V_{bd} \quad (22)$$

$$\dot{I}_{bq} = \frac{1}{L_b} V_{nq} - \frac{R_b}{L_b} I_{bq} - \omega_s I_{bd} - \frac{1}{L_b} V_{bq} \quad (23)$$

$$\dot{V}_{cd} = \frac{1}{C} I_{d1} + \omega_s V_{cq} \quad (24)$$

$$\dot{V}_{cq} = \frac{1}{C} I_{q1} - \omega_s V_{cd} \quad (25)$$

As a result, aforementioned model can be written as a set of nonlinear first order ordinary differential equations. The control parameter for these equations is the compensation factor ($\mu = X_C / X_L$). Consequently, bifurcation theory will be used to nonlinear model that can be described in the following form:

$$\dot{X} = F(X, U; \mu) \quad (26)$$

where X is a state variables vector, X_1, X_2, …, X_n, n is an integer number, U is the input vector, F is the field vector and μ is the system bifurcation parameter which is in this study is the transmission line compensation degree.

The following are the state variables of the considered power system: $X_1 = \omega_t$, $X_2 = \delta_{tg}$, $X_3 = \omega_g$, $X_4 = I_{ds}$, $X_5 = I_{qs}$, $X_6 = E_{d1}$, $X_7 = E_{q1}$, $X_8 = E_{d2}$, $X_9 = E_{q2}$, $X_{10} = V_{ds}$, $X_{11} = V_{qs}$, $X_{12} = I_d$, $X_{13} = I_q$, $X_{14} = I_{md}$, $X_{15} = I_{mq}$, $X_{16} = I_{nd}$, $X_{17} = I_{nq}$, $X_{18} = V_{md}$, $X_{19} = V_{mq}$, $X_{20} = V_{nd}$, $X_{21} = V_{nq}$, $X_{22} = I_{bd}$, $X_{23} = I_{bq}$, $X_{24} = V_{cd}$, $X_{25} = V_{cq}$, and the inputs are: $U_1 = T_w$, $U_2 = V_{bd}$, $U_3 = V_{bq}$.

Equations (1)-(25) show a full description to the dynamics of the system. The fixed point (equilibrium solution) can be calculated by placing zero to the derivatives of the state variables of the considered system. The system steady state stability can be determined by inspection of the Jacobian matrix eigenvalues of the equations calculated at the equilibrium point. System eigenvalues are calculated for a broad range of series compensation degrees in the cases of different levels of wind farm sizes and different levels of wind farm power output using MATLAB software R2016b.

As the bifurcation parameter varies, up to a critical value of compensation (Hopf bifurcation point), the system will loss stability. Consequently, the system oscillates subsynchronously and a small limit cycle attractor is born at HB point. The type of this point is obtained by numerical integration of the system after applying small value of initial disturbances, slightly after and before the bifurcation point.

4. Numerical Simulations and Results

In this part, numerical simulation results depend on the full nonlinear dynamical mathematical model are obtained. The dynamics of the considered model are described by Equations (1)-(25). The equilibrium solutions (operating points) at any value of compensation factor (μ) are given by placing zero to the derivatives of the 25 state variables in the system. Then by testing of the Jacobian matrix eigenvalues evaluated at the equilibrium point, the stability of the operating solution is obtained. Bifurcations of SSR are examined for different levels of series compensation and various wind farm outputs. The compensation level ($\mu = X_C/X_L$) is varied between zero to 1; whereas, the wind farm power outputs is taking the values from 100 MW to 600 MW.

The model eigenvalues are calculated for a broad range of compensation degrees in the cases of different levels of wind farm sizes and different values of wind farm output using the MATLAB software. In this study, there is one real eigenvalue and 24 complex conjugate eigenvalues. The real eigenvalue is always negative and indicates the field windings of the IG (monotonic mode). The 24 complex conjugate eigenvalues create 12 oscillatory modes. At this stage, only selected modes will be taken into consideration, which are monotonic mode, supersynchronous electrical mode, subsynchronous electrical mode, electro-mechanical modes (for first rotor and second rotor) and trosional modes. More specifically, the focus in this research is on the subsynchronous electrical mode and when this mode interacts with the torsional modes. When these interactions happen, the torsional modes may become self-excited and this is a

worrisome problem. This problem end with fatigue and finally damage to the rotor, despite it has small amplitudes. Some interactions may not be strong enough to change the system to instability. In contrary interactions, they are strong enough to transfer the real parts of the eigenvalues from left- to the right- half of the complex plane, for which a Hopf bifurcation take places.

4.1 Variation Based on Wind Farm Size

The case of different sizes of wind farms (100 MW to 600 MW rated wind farms) with an enormous range of series compensation values is investigated. The equilibrium point stability is determined by inspection the eigenvalues of the linearized system. For the case of 300 MW rating size of wind farm, the outcomes indicate that the equilibrium point loses stability at μ=HB=0.8865. Figure 3 indicates the equilibrium point stability regions in δ_g–μ plane. The considered system has stable equilibrium point in the range 0<μ<HB=0.8865, unstable equilibrium point in the range HB=0.8865<μ≤1 and supercritical Hopf bifurcation point at μ=HB=0.8865. Consequently, a stable limit cycle with small-amplitude is born at HB point.

Figure 4 presents the time history of the system after applying 1% initial disturbance on the Electromagnetic torque output of generator at μ=0.8750, which is less than HB resulted in a stable system. On the other hand, Fig. 5 indicates the system time history with 1% initial disturbance in the electromagnetic torque output of generator at μ=0.8970, which is greater than HB. Here, the system transfers to a periodic solution resulting in oscillations with a supercritical Hopf bifurcation. Therefore, a stable periodic solution is emanated at the bifurcation point.

For the case of 600 MW rating size of wind farm, the outcome confirms that the equilibrium point loses stability at μ=HB=0.9215. Figure 6 shows the equilibrium point stability regions in δ_g–μ plane. Here, the system has stable equilibrium point in the range 0<μ<HB=0.9215, unstable equilibrium point in the range HB=0.9215<μ≤1 and a supercritical Hopf bifurcation point at μ=HB=0.9215. Thus, a limit cycle is located at μ=HB.

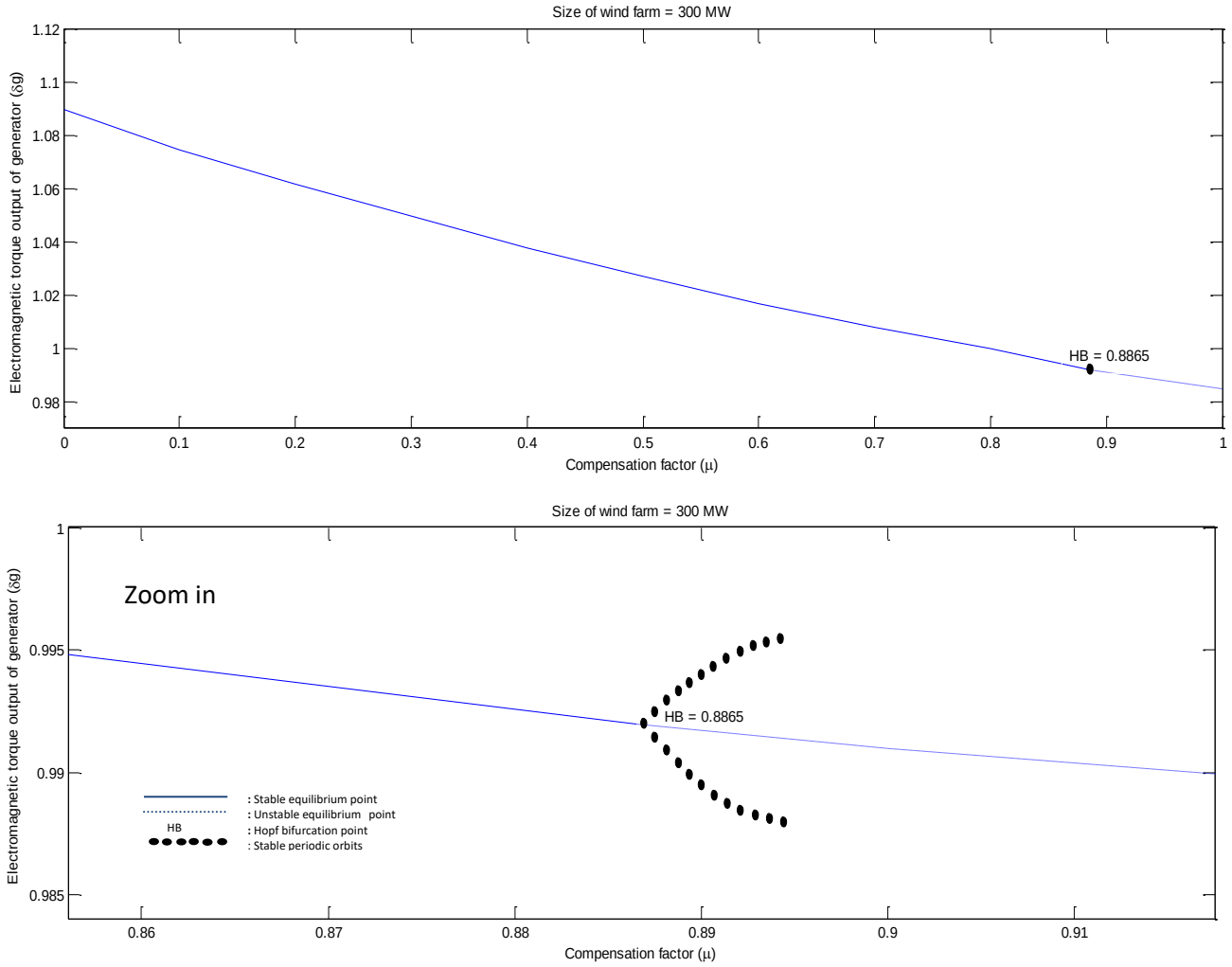

Fig. 3. Bifurcation diagram presenting variation of the Electromagnetic torque output of generator δ_g with the compensation factor μ (for the case of 300 MW rating size of wind farm).

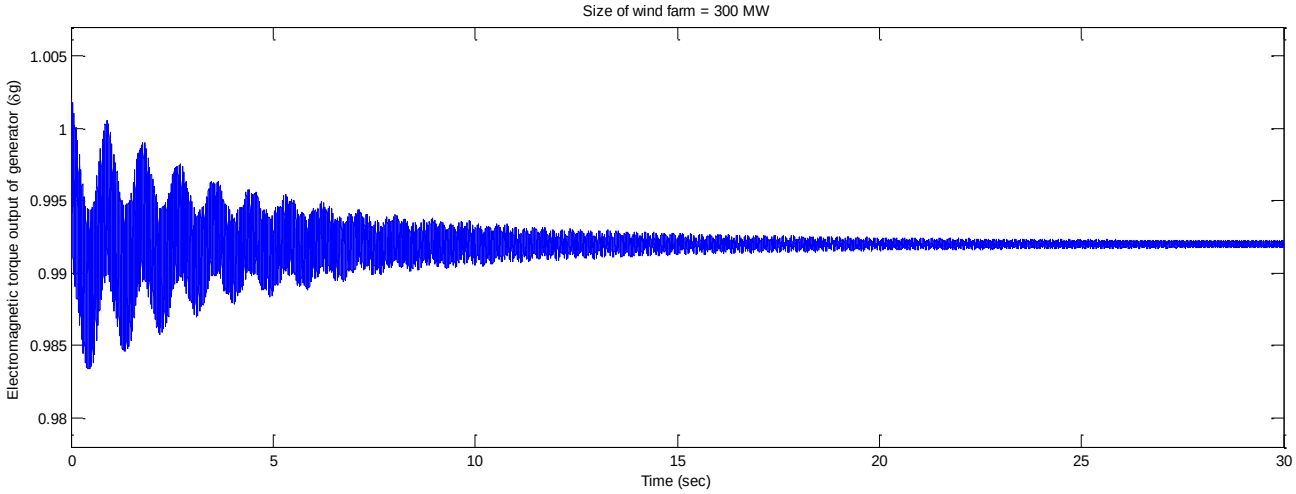

Fig. 4. Electromagnetic torque output of generator δ_g at μ=0.8750 (for 300 MW rating size of wind farm).

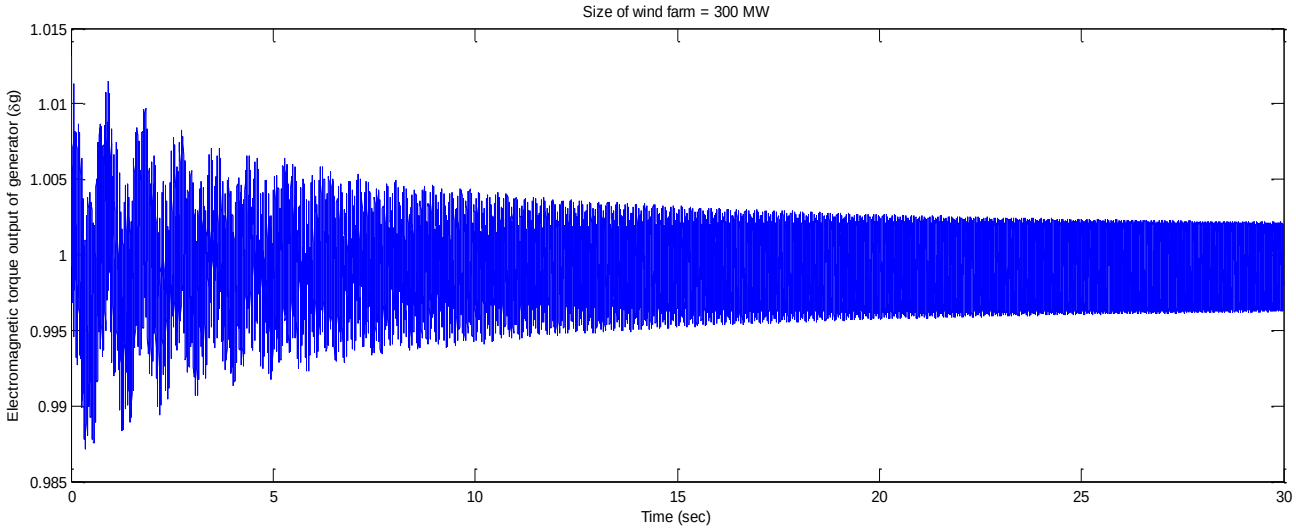

Fig. 5. Electromagnetic torque output of generator δ_g at μ=0.8970 (for 300 MW rating size of wind farm).

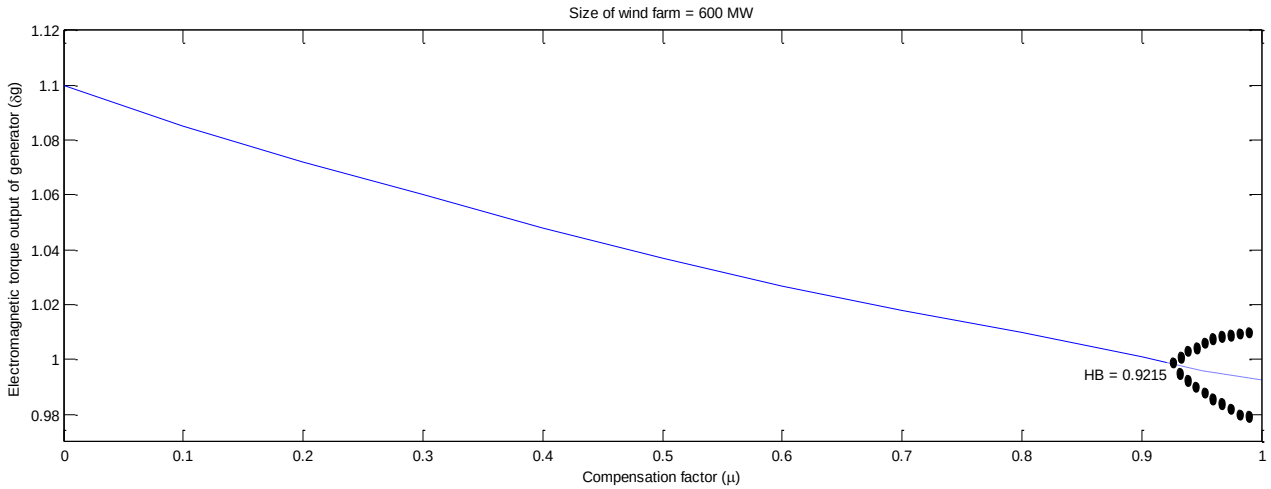

Fig. 6. Bifurcation diagram presenting variation of the Electromagnetic torque output of generator δ_g with the compensation factor μ (for 600 MW rating size of wind farm).

Table 1 shows the type and level of the Hopf bifurcation points for various sizes of wind farm. The Hopf bifurcation point firstly shifts to the left at a less value of compensation (for the cases of 100, 200 and 300 MW rating), then shifts to the right at a larger value of compensation (for the cases of 400, 500 and 600 MW rating). For all cases, the type of Hopf bifurcation does not change and sets as supercritical and a limit cycle is located at μ=HB. Therefore, the results show that the variation of Hopf bifurcation caused by varying the size of wind farm is fundamentally a quantitative change.

Table 1. Type and level of the Hopf bifurcation points for various sizes of wind farm.

Size of wind farm (MW rating)	Hopf bifurcation point (HB = μ_c)	Type of the Hopf bifurcation
100	0.9305	supercritical
200	0.9135	supercritical
300	0.8865	supercritical
400	0.8985	supercritical
500	0.9060	supercritical
600	0.9215	supercritical

4.2 Variation based on Wind Farm Output

A large wind farm of 600 MW with an enormous range of series compensation values is considered for this analysis whose output power is variable. The wind farm produces variable output power because of the variation based on wind speed. For the case of 300 MW power output of 600 MW, the equilibrium point stability range in the δ_g–μ plane including HB point are shown in Fig. 7. It can be observed that there are stable equilibrium point to the left of HB=0.9320 and unstable equilibrium point to the right of HB=0.9320. The equilibrium point loses stability at a Hopf bifurcation point. A couple of complex conjugate eigenvalues moves in this situation from the left half complex plane to the right half one.

Figure 8 indicates the time history of the system after applying 1% initial disturbance on the Electromagnetic torque output of generator at μ=0.9450 which is greater than HB leading to unstable system. The time history of the system is obtained by numerical integration after applying small disturbance before the HB to examine if the limit cycles that created resultantly of the HB are stable or unstable. Figure 9 indicates the time history of the system after applying 1% initial disturbance on the Electromagnetic torque output of generator at μ=0.9240, which is less than HB, also leading to an unstable system. Consequently, subcritical Hopf bifurcation is located. Hence, an unstable periodic solution is emanated at this point.

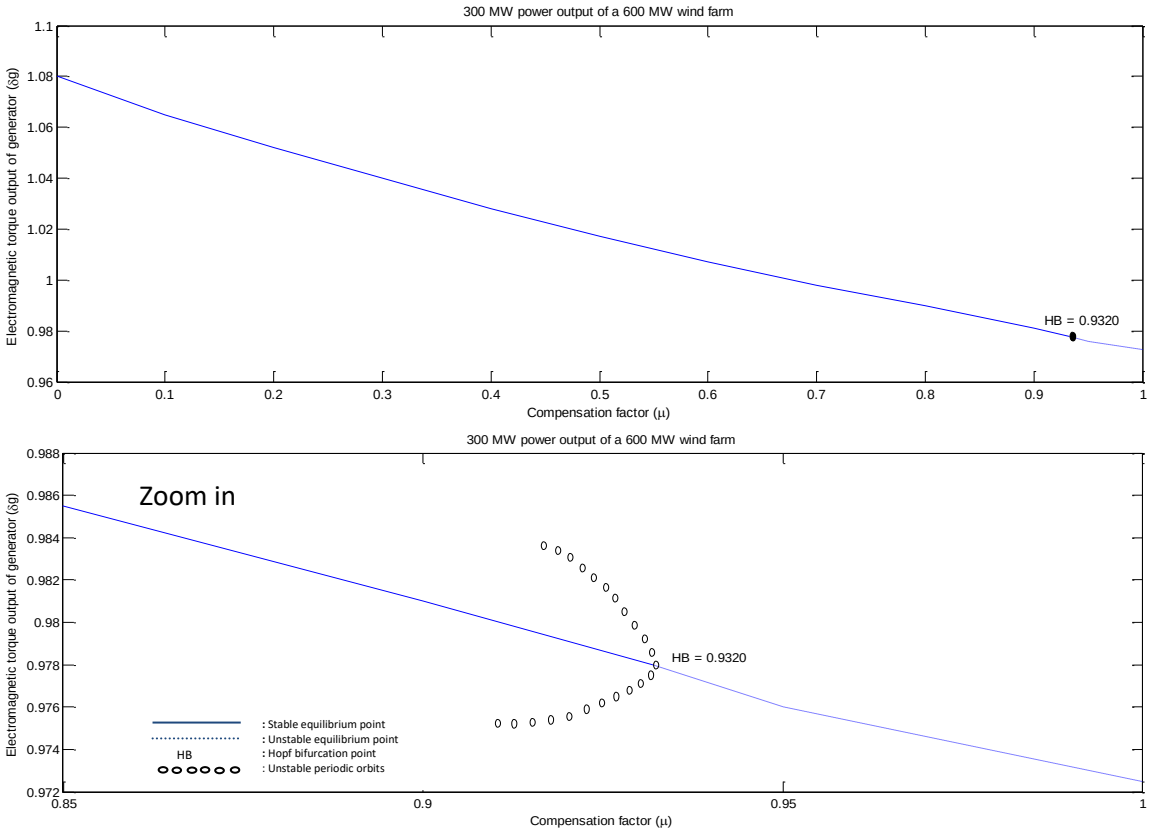

Fig. 7. Bifurcation diagram presenting variation of the Electromagnetic torque output of generator δ_g with the compensation factor μ (for 300 MW power output of 600 MW).

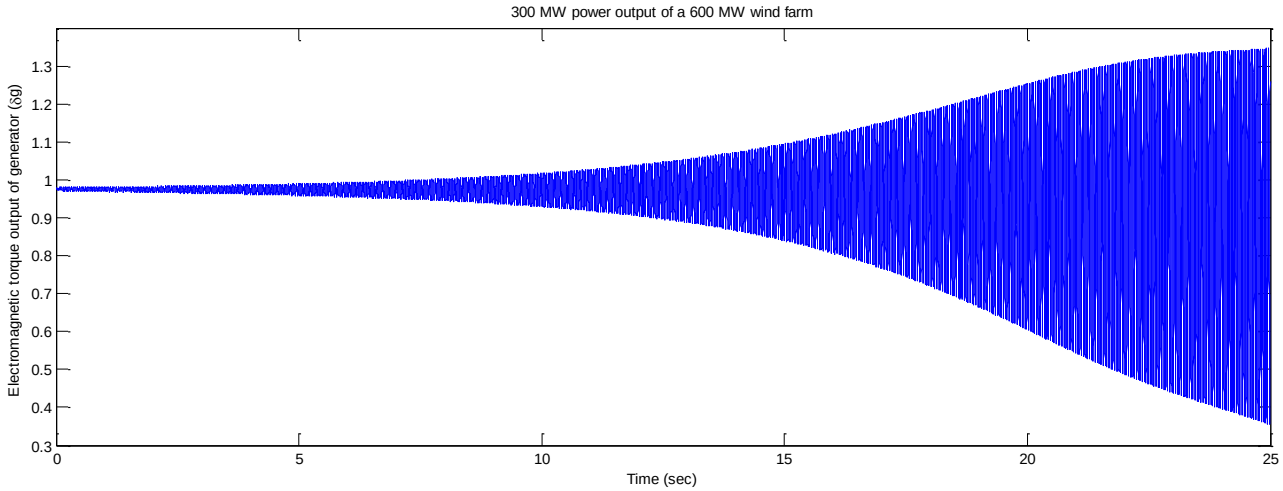

Fig. 8. Electromagnetic torque output of generator δ_g with the compensation factor μ (for 300 MW rating size of wind farm and at μ=0.9450).

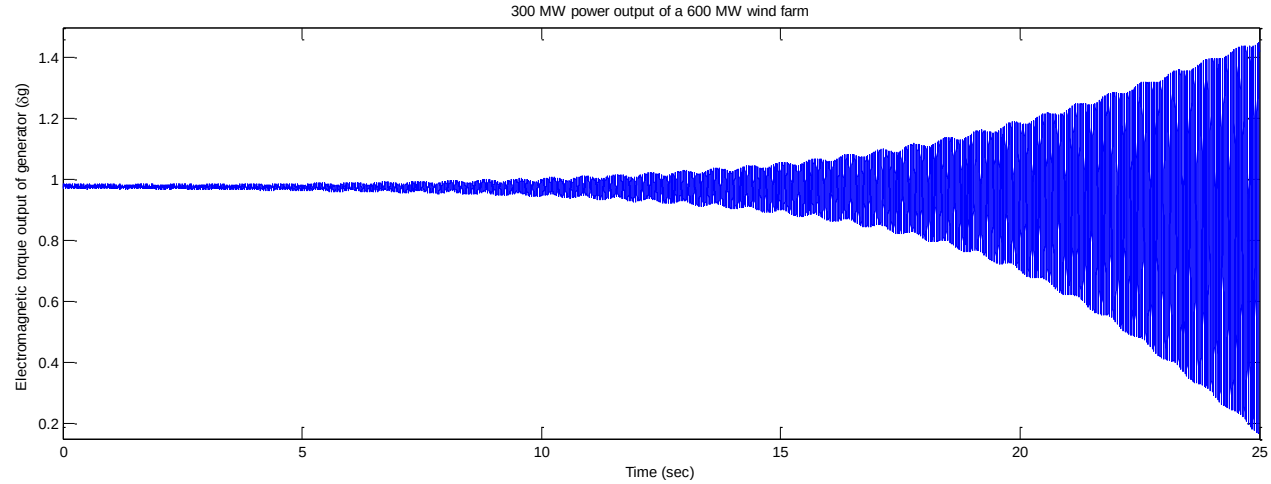

Fig. 9. Electromagnetic torque output of generator δ_g with the compensation factor μ (for 300 MW rating size of wind farm and at μ=0.9240).

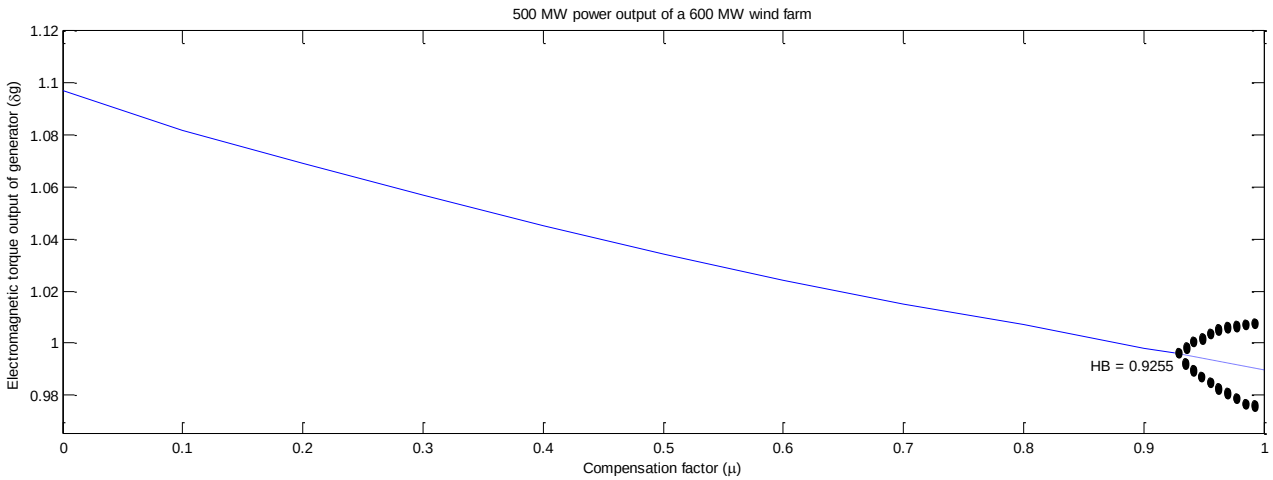

Fig. 10. Bifurcation diagram presenting variation of the Electromagnetic torque output of generator δ_g with the compensation factor μ (for 500 MW power output of 600 MW).

For the case of 500 MW power output of 600 MW, the equilibrium point stability range in the δ_g–μ plane including a HB point are presented in Fig. 10. It can be noticed that a stable equilibrium point is located to the left of HB=0.9255 and an unstable equilibrium point to the right of HB=0.9255. The equilibrium point loses stability at HB. A couple of complex conjugate eigenvalues moves in this case from left half complex plane to right one for which the Hopf bifurcation point changes to supercritical.

Table 2 shows the type and level of the Hopf bifurcation points for various wind farm power outputs. Here, the Hopf bifurcation point shifts a little to the left at a slightly less value of compensation when a large wind farm power output increases. The type of Hopf bifurcation changes from subcritical to supercritical. Therefore, it can be concluded that the conversion of Hopf bifurcation created by varying the output power is basically qualitative with some quantitative modification.

Table 2. Type and level of the Hopf bifurcation points for various wind farm power outputs

Power output in MW of a 600 MW	Hopf bifurcation point (HB = μ_c)	Type of the Hopf bifurcation
100	0.9375	subcritical
200	0.9345	subcritical
300	0.9320	subcritical
400	0.9295	supercritical
500	0.9255	supercritical
600	0.9215	supercritical

5. Conclusion

In this study, bifurcations of subsynchronous resonance in power systems containing induction generator have been discussed. The system consisting of wind farms liked with series compensated lines. The consequence of series compensation levels, wind power output, and size of wind farm on bifurcation has been investigated. For the cases of fixed sizes of wind turbine and fixed power output and when the level of compensation system increase, the system loses stability at a HB point. This is because the system tends to become less stable when the compensation value is increased. As the size of wind farm increase, the Hopf bifurcation point crosses to the left first at a less value of compensation then it moves to the right at a larger value of compensation. This is due to the fact that when the size of the wind farm is increased at a fixed compensation value, initially the electrical mode tends to be less stable but later becomes more stable. The type of Hopf bifurcation is supercritical in all cases. For large 600 MW wind farm, the impact of variation of the power output on bifurcation is mainly qualitative change. As the wind farm power output increases, the Hopf bifurcation point will move a little to the left at a slightly less value of compensation. This is because the effect of power output on the stability of electrical mode is found to be quite negligible. In this case, the type of Hopf bifurcation alternates from subcritical to supercritical type.

It can be concluded that the level of bifurcations affected by the wind farm size whereas the type of bifurcations depends on the wind farm power output. Consequently, the influence of changing the wind farm size on bifurcation is only a quantitative change, whereas the effect of variation in the power output is principally a qualitative change. The stable region for a large wind farm generating a smaller power output is more stable than smaller wind farm generating same output power. This means 200 MW power output of a 600MW wind farm is more stable than 200 MW rating of wind farm. As a future work, Flexible AC Transmission System (FACTS) controllers may be utilized to control bifurcations of nonlinear dynamical systems. FACTS controllers has several advantages for a power system such as damping power oscillations, decreasing subsynchronous resonance, and controlling power flow in the line.

References

[1] R. K. Varma, S. Auddy, “Mitigation of Subsynchronous Oscillations in a Series Compensated Wind Farm with Static Var Compensator”, IEEE, 2006.

[2] A. Daghigh, H. Javadi, H. Torkaman, “Considering Wind Speed Characteristics in the Design of a Coreless AFPM Synchronous Generator”, International Journal of Renewable Energy Research (IJRER), Vol 6, No 1, 2016.

[3] R. Campaner, M. Chiandone, G. Sulligoi, F. Milano, “Automatic voltage and reactive power control in distribution systems: Dynamic coupling analysis”, 2016 IEEE International Conference on Renewable Energy Research and Applications (ICRERA), 20 Nov - 23 Nov 2016, Birmingham, United Kingdom, IEEE Conference Publications, pp. 934 – 939.

[4] M. H. Baloch, J. Wang, G. S. Kaloi, “A Review of the State of the Art Control Techniques for Wind Energy Conversion System”, International Journal of Renewable Energy Research (IJRER), Vol 6, No 4, 2016.

[5] I. G. Adebayo; A. A. Jimoh; A. A. Yusuff, “Identification of suitable nodes for the placement of reactive power compensators”, 2016 IEEE International Conference on Renewable Energy Research and Applications (ICRERA), 20 Nov - 23 Nov 2016, Birmingham, United Kingdom, IEEE Conference Publications, pp. 645 - 649.

[6] M. R. Wani, M. A. Wani; R. Riyaz, “Cluster based approach for mining patterns to predict wind speed”, 2016 IEEE International Conference on Renewable Energy Research and Applications (ICRERA), 20 Nov

- 23 Nov 2016, Birmingham, United Kingdom, IEEE Conference Publications, pp. 1046 - 1050.

[7] M. Alivirdizadeh, B. Tousi, H. Ghahramani, J. Khazaie, S. Rajebi, "A Novel Damping Controller for Inter-Area Oscillation by Means of DFIG-Based Wind Farm", International Journal on Technical and Physical Problems of Engineering (IJTPE), Issue 8, Vol. 3, No. 3, pp. 118-124, September 2011.

[8] S. Dolatabadi, S. Tohidi, "A Review on Position Sensorless Methods for Wind Generators", International Journal of Renewable Energy Research (IJRER), Vol 7, No 2, 2017.

[9] S. M. Vaca; C. Patsios, P. Taylor, "Enhancing frequency response of wind farms using hybrid energy storage systems", 2016 IEEE International Conference on Renewable Energy Research and Applications (ICRERA), 20 Nov - 23 Nov 2016, Birmingham, United Kingdom, IEEE Conference Publications, pp. 325 - 329.

[10] American Wind Energy Association. [Online] http://www.awea.org/, January 2017.

[11] V. Oleschuk, V. Ermuratskii, F. Blaabjerg, "Six-phase vehicular drive with renewable dc sources and hybrid PWM control of four inverters", 2015 International Conference on Renewable Energy Research and Applications (ICRERA), 22-25 November 2015, Palermo, Italy, IEEE Conference Publications, pp. 515 - 519.

[12] Wind force 12, European Wind Energy Association. [Online] http://www.ewea.org/, January 2017.

[13] P. Kundur, "Power System Stability and Control", New York, McGraw-Hill, 1994.

[14] L.A.S. Pilotto, A. Bianco, W.F. Long, A. Edris, "Impact of TCSC Control Methodologies Subsynchronous Oscillations", IEEE Transactions on Power Delivery, Vol. 18, No. 1, pp. 243-252, January 2003.

[15] D. Raii, S. Faried, G. Ramakrishna, A. Edris, "Hybrid series compensation scheme capable of damping subsynchronous resonance". IET Generat. Transm. Distrib. 2010, 4, 456–466.

[16] F.D. De Jesus, E.H. Watanabe, L.F.W. De Souza, J.E.R. Alves, Jr., "SSR and Power Oscillation Damping Using Gate-Controlled Series Capacitors (GCSC)", IEEE Transactions on Power Delivery, Vol. 22, No. 3, pp. 1806-1812, July 2007.

[17] A. H. Nayfeh, and B. Balachandran, , 1995, Applied Nonlinear Dynamics, Wiley, New York.

[18] P. Pourbeik, R.J. Koessler, D.L. Dickmander and W. Wong, "Integration of Large Wind Farms into Utility Grids (Part 2 - Performance Issues)", in Proc. 2003 IEEE PES GM, pp. 1520-1525.

[19] A. Ostadi, A. Yazdani, and R. K. Varma, "Modeling and Stability Analysis of a DFIG-Based Wind-Power Generator Interfaced With a Series-Compensated Line," IEEE Trans. on Power Delivery, vol. 24, no. 3, pp. 1504-1514, Jul. 2009.

[20] L. Fan, R. Kvasseri, Z. Lee Miao and C. Zhu, "Modeling of DFIG-Based Wind Farms for SSR Analysis," IEEE Trans. on Power Delivery, vol. 25, no. 4, pp. 2073-2082, Oct. 2010.

[21] L. Fan, C. Zhu, Z. Miao, M. Hu, "Modal Analysis of a DFIG-Based Wind Farm Interfaced With a Series Compensated Network," IEEE Trans. on Energy Conversion, vol. 26, no. 4, pp. 1010-1020, Dec. 2011.

[22] G. D. Irwin, A. K. Jindal, and A. L. Isaacs, "Sub-synchronous control interactions between type 3 wind turbines and series compensated AC transmission systems," in Proc. 2011 IEEE PES GM, pp. 1-6.

[23] L. Fan, and Z. Miao, "Mitigating SSR Using DFIG-Based Wind Generation," IEEE Trans. on Sustainable Energy, vol. 3, no. 3, pp. 349-358, Jul. 2012.

[24] Y. Song, X. Wang, & F. Blaabjerg, "High Frequency Resonance Damping of DFIG based Wind Power System under Weak Network", IEEE Transactions on Power Electronics, April 2016.

[25] Zhao Bin, Li Hui, Wang Mingyu, Chen Yaojun, Liu Shengquan, Yang Dong, Yang Chao, Hu Yaogang, Chen Zhe, "An active power control strategy for a DFIG-based wind farm to depress the subsynchronous resonance of a power system", International Journal of Electrical Power & Energy Systems, Vol. 69, pp. 327 – 334, July 2015.

[26] B. Zhao, H. Li, M. Wang, Y. Chen, S. Liu, D. Yang, C. Yang, Y. Hu, Z. Chen, "An Optimal Reactive Power Control Strategy for a DFIG-Based Wind Farm to Damp the Sub-Synchronous Oscillation of a Power System", 7 (5): 3086-3103, Energies. 2014.

[27] A.A. Tanvir, A. Merabet, R. Beguenane, "Real-Time Control of Active and Reactive Power for Doubly Fed Induction Generator (DFIG)-Based Wind Energy Conversion System". 8 (9): 10389-10408. Energies. 2015.

[28] A.H. Nayfeh and B. Balachandran, Applied Nonlinear Dynamics, Wiley, New York, 1995.

[29] IEEE Committee Report, "Second Benchmark Model for Computer Simulation of Subsynchronous Resonance," IEEE Trans. on Power Apparatus and Systems, vol. PAS-104, no. 5, pp. 1057-1066, May 1985.

[30] T. Petru and T. Thiringer, "Modeling of wind turbines for power system studies," IEEE Trans. on Power Systems, vol. 17, no. 4, pp. 1132- 1139, Nov. 2002.

[31] F. Mei, and B. Pal, "Modal Analysis of Grid-Connected Doubly Fed Induction Generators," IEEE Transactions on Energy Conversion, vol. 22, no. 3, pp. 728-736, Sep. 2007.

[32] B. Pal and F. Mei, "Modelling adequacy of the doubly fed induction generator for small-signal stability studies in power systems," IET Renewable Power Generation, vol. 2, no. 3, pp. 181-190, Sep. 2008.

[33] R. K. Varma, S. Auddy and Y. Semsedini, "Mitigation of Subsynchronous Resonance in a Series-Compensated Wind Farm Using FACTS Controllers," IEEE Trans. on Power Delivery, vol. 23, no. 3, pp. 1645-1654, Jul. 2008.

Appendix A

Physical clarifications for the parameters of the system are presented in this appendix. The parameters are classified as follows:

1) Two-mass Drive Train System parameters:

ω_t: Wind turbine angular speed (rad/s).

δ_{tg}: Torsional angle between generator and wind turbine (rad).

ω_g: Generator angular speed (rad/s).

T_w : Wind turbine mechanical torque input to (pu).

T_g : Generator electromagnetic torque output (pu), where : $T_g = E_{d1}\, I_{ds} + I_{qs}\, E_{q1}$

D_t : Wind turbine damping coefficient (pu).

D_g : Generator damping coefficient of (pu).

H_g: Generator Inertia constant.

H_t: Wind turbine inertia constant.

K_{tg}: Shaft stiffness between generator and wind turbine.

D_{tg}: Damping coefficient between generator and wind turbine.

2) Induction generator parameters:

I_{ds}, I_{qs} : *d-q* components of stator current of double-cage induction generator.

V_{ds}, V_{qs} : *d-q* components of voltage at the generator terminal.

E_{d1}, E_{q1} : *d-q* components of induced rotor voltages across first-cage of double-cage IG.

E_{d2}, E_{q2}: *d-q* components of induced rotor voltages across second-cage of double-cage IG.

X_m: Mutual reactance between the rotor and stator windings.

X_{ro1}: Per phase first-cage rotor leakage reactance.

X_{ro2}: Per phase second-cage rotor leakage reactance.

R_{r1}: Per phase first-cage rotor resistance.

R_{r2}: Per phase second-cage rotor resistance.

R_s : Per phase stator resistance.

X_{so} : Per phase stator leakage reactance.

3) Transmission lines (network) parameters:

V_{ds}, V_{qs}: *d-q* components of wind turbine terminal voltage (pu).

I_d, I_q: *d-q* components of current from wind farm to bus (pu).

I_{d1}, I_{q1} : *d-q* components of first transmission line current (pu).

I_{d2}, I_{q2} : *d-q* components of second transmission line current (pu).

V_{md}, V_{mq}: *d-q* components voltage at bus-m (pu).

V_{nd}, V_{nq}: *d-q* components voltage at bus-n (pu).

I_{bd}, I_{bq}: *d-q* components current from bus-n to infinite bus (pu).

V_{cd}, V_{cq}: Series capacitor *d-q* components voltage (pu).

V_{bd}, V_{bq}: Infinite bus *d-q* components voltage (pu).

H_g: Generator Inertia constant.

H_t: Wind turbine Inertia constant.

K_{tg}: Shaft stiffness between generator and wind turbine.

D_{tg}: Damping coefficient between generator and wind turbine.

C_g : The capacitor for power factor correction at generator terminal of wind turbine.

R_t : Transformer winding resistance.

L_t : Leakage inductance of transformer winding.

R_1 : Resistance of AC transmission line-1.

L_1: Inductance of AC transmission line-1.

R_2 : Resistance of AC transmission line-2.

L_2 : Inductance of AC transmission line-2.

C_m : Fictitious shunt capacitance at bus-m.

C_n : Fictitious shunt capacitance at bus-n.

R_b : Resistance of infinite bus.

L_b: Inductance of infinite bus.

X_c : The reactance of the series capacitor (pu).

X_1 : Transmission line-1 reactance (pu).

f_e : The nominal frequency of the power system (Hz).

f_r : The frequency of induction generator rotor (Hz).

ω_s : Synchronous angular frequency (rad/s).

ω_r : Induction generator angular frequency (rad/s).

S : Slip of induction generator.

μ : Series compensation level.

Appendix B

Numerical values of the system parameters are as follows:

1) Two-mass Drive Train System parameters:

H_t = 4 s , H_g = 0.75 s ,

K_{tg} = 0.2 pu/el.rad , D_{tg} = 1.5 pu.

2) Induction generator parameters:

X_{rm} = 3.8892 pu , X_m = 0.00506 pu ,

X_{ro2} = 0.072175 pu , X_{ro1} = 0.21172 pu ,

R_{r2} = 0.01923 pu , R_{r1} = 0.01199 pu ,

R_s = 0.00506 pu , X_{so} = 0.13176 pu .

Where:

$X_{1\_2} = X_m + X_{rm}$, $X_s = X_{so} + X_m$,

$X_{r1} = X_{ro1} + X_{1\_2}$, $X_{r2} = X_{ro2} + X_{1\_2}$,

$X_r = X_{r1}X_{r2} - X_{1\_2}^2$, $X_o = X_s - \frac{X_m^2 X_{ro2}}{X_r}$.

3) Transmission lines (network) parameters:

p_{base} = 2.3 MW , V_{base} = 690 V ,

f_e = 60 Hz , $C_g = 2 \times 10^{-6}$ F ,

R_t = 0.0002 pu , $L_t = \frac{0.02}{2\pi f_r}$ pu ,

R_1 = 0.0074 pu , $L_1 = \frac{0.08}{2\pi f_r}$ pu ,

R_2 = 0.0067 pu , $L_2 = \frac{0.0739}{2\pi f_r}$ pu ,

$C_m = 2000 \times 10^{-6}$ F , $C_n = 2000 \times 10^{-6}$ F,

R_b = 0.0014 pu , $L_b = \frac{0.03}{2\pi f_r}$ pu .

where:

$X_1 = 2\pi f_r L_1$, $X_c = \mu X_1$,

$f_{cr} = f_e \sqrt{\frac{X_c}{X_1}}$, $f_r = f_e - f_{cr}$,

$\omega_s = 2\pi f_e$, $\omega_r = 2\pi f_r$, $S = \frac{(\omega_s - \omega_r)}{\omega_s}$